

Three-dimensional carbon Archimedean lattices for high-performance electromechanical actuators

Nguyen T. Hung^{a,*}, Ahmad R. T. Nugraha^a, Riichiro Saito^a

^a*Department of Physics, Tohoku University, Sendai 980-8578, Japan*

Abstract

We propose three-dimensional carbon (3D-C) structures based on the Archimedean lattices (ALs) by combining sp^2 bonding in the polygon edges and sp^3 bonding in the polygon vertices. By first-principles calculations, four types of 3D-C ALs: $(4, 8^2)$, $(3, 12^2)$, (6^3) , and (4^4) 3D-Cs are predicted to be stable both dynamically and mechanically among 11 possible ALs, in which the notations (p_1, p_2, \dots) are the indices of the AL structures. Depending on their indices, the 3D-C ALs show distinctive electronic properties: the $(4, 8^2)$ 3D-C is an indirect band-gap semiconductor, the $(3, 12^2)$ 3D-C is semimetal, while the (6^3) and (4^4) 3D-Cs are metals. Considering the structural deformation due to the changes in their electronic energy bands, we discuss the electromechanical properties of the 3D-C ALs as a function of charge doping. We find a semiconductor-to-metal and semimetallic-to-semiconductor transitions in the $(4, 8^2)$ and $(3, 12^2)$ 3D-Cs as a function of charge doping, respectively. Moreover, the $(3, 12^2)$ 3D-C exhibits a sp^2 - sp^3 phase transformation at high charge doping, which leads to a huge 30% irreversible strain, while the reversible strain in the $(4, 8^2)$ 3D-C is up to 9%, and thus they are quite promising for electromechanical actuators.

1. Introduction

Scientific and technological attempts to design and synthesize actuation materials as a building block of artificial muscle have been quite intensive during the past two decades, with wide potential applications in biometric machines, robotics, and medical sciences [1, 2, 3, 4]. Such an actuation material based on carbons was proposed by Baughman et al. in 1999, who synthesized carbon nanotube (CNT) yarn and demonstrated that CNT yarn can generate *stress* 100 times that achievable by natural muscles (~ 0.35 MPa) [5]. Following this initial demonstration, many studies have sought other carbon actuator materials such as single, multilayer graphene, graphene oxide, graphitic carbon nitride, and CNT films via both experimental and theoretical approaches [6, 7, 8, 9, 10, 11, 12]. However, both CNT yarn and graphene showed a small *strain* of about 1% under charge (electron or hole) doping [13, 14], while the skeletal muscles provide a work cycles involving contractions of more than 20%. The CNT yarn or the multilayer graphene are also formed by the weak van der Waals (vdW) forces, which lead to a possible mechanical failure along the direction of the vdW interactions in these material [14]. To overcome this problem, we may use such CNT and graphene structures to form new three-dimensional carbon (3D-C) materials that still inherit their superb properties while simultaneously avoiding vdW interaction between different tubes or layers.

Carbon is one of the most versatile elements due to its ability to form sp -, sp^2 -, and sp^3 -hybridized bonds, resulting in various allotropes that have already been experimentally identified, such as graphite, diamond, fullerene, CNT, and

graphene [15]. Recently, computational modeling based on the first-principles density functional theory (DFT) and molecular dynamics opens the possibility to predict more carbon allotropes. Some new 3D-C materials, such as 3D-C honeycomb [16], T-carbon [17], Y-carbon [18], L-carbon [19], and cubane-based 3D porous carbon [20] have been either observed or proposed, where all these materials are found to be dynamically, mechanically, and thermally stable. Furthermore, the elastic constants of some of these 3D-C structures were studied. Zhao et al. [21] showed that 3D-C structures have large Young's moduli, large tensile strength, and low density. Recently, experimentalists have successfully synthesize a kind of 3D-C structures in forms of carbon honeycomb by deposition of vacuum-sublimated graphite [22] and nanoporous carbon made by buckybowl-like nanographene [23]. This fact shows a great potential in designing the 3D-C materials and structures while retaining low density and excellent mechanical properties for electromechanical actuators. In this sense, a systematic theoretical design could be the first step to suggest possible structures suitable as electromechanical actuators so that experimentalists can synthesize the recommended structures.

Inspired by the structure of the Archimedean lattices (ALs), defined as a complete set of lattices having all vertices are equivalent, we design a class of 3D-Cs by a combination of sp^2 bonding in the polygon edges and sp^3 bonding in the polygon vertices. In this work, considering efficient computational time, 4 of 11 possible 3D-C ALs are calculated using the first-principles DFT calculations. Hereafter, the 4 possible 3D-C ALs are referred to as $(4, 8^2)$, $(3, 12^2)$, (6^3) , and (4^4) 3D-Cs, in which the notations (p_1, p_2, \dots) are the indices of the AL structures based on the types of polygons connected at a given vertex (see Fig. 1a). We find that these 3D-C ALs are both dy-

*Corresponding author. Tel.: +81 22 795 7754; Fax: +81 22 795 6447.

Email address: nguyen@flex.phys.tohoku.ac.jp (Nguyen T. Hung)

namically and mechanically stable because all of their phonon frequencies and mechanical stability conditions are positive, respectively. We will discuss the electromechanical properties of the 3D-C ALs as a function of charge doping, for both electron and hole doping cases, by considering the structural deformation due to the changes in their electronic energy bands. Three important physical phenomena in the doped 3D-C ALs are found from the calculations: (1) a semiconductor-to-metal and semimetallic-to-semiconductor transitions in the $(4, 8^2)$ and $(3, 12^2)$ 3D-Cs, respectively, (2) a structural transformation between sp^2 - sp^3 phases under heavy doping in the $(3, 12^2)$ 3D-C, and (3) a large change of reversible strain up to 5%, essential for the artificial muscle applications.

2. Calculation methods

We perform first-principles calculations to determine the total energy and the electronic structure of the 3D-C ALs using Quantum ESPRESSO [24]. The Rabe-Rappe-Kaxiras-Joannopoulos ultrasoft pseudopotential with an energy cutoff of 60 Ry is chosen for the expansion of the plane waves [25]. Note that the choice of 60 Ry energy cutoff is sufficient for converging the total energy calculation. The exchange-correlation energy is evaluated by the general-gradient approximation using the Perdew-Burke-Ernzerhof (PBE) function [26]. In our simulation, the \mathbf{k} -point grids in the Brillouin-zone are employed according to the Monkhorst-Pack scheme, where \mathbf{k} is the electron wave vector. $9 \times 9 \times 13$, $5 \times 5 \times 13$, $7 \times 7 \times 9$, and $16 \times 16 \times 6$ \mathbf{k} -points are used for $(4, 8^2)$, $(3, 12^2)$, (6^3) , and (4^4) 3D-Cs, respectively. To obtain optimized atomic configurations of 3D-C ALs, the atomic positions and cell vectors are fully relaxed using the Broyden-Fletcher-Goldfarb-Shanno minimization method [27, 28, 29, 30] until all the Hellmann-Feynman forces and all components of the stress are less than $5e^{-4}$ Ry/a.u. and $5e^{-2}$ GPa, respectively, which are adequate for the present work. To examine the dynamically stable of the 3D-C ALs, phonon dispersions are computed using the density functional perturbation theory (DFPT) within the linear response approximation [31]. The dynamical matrices are calculated on a $4 \times 4 \times 6$, $2 \times 2 \times 6$, $3 \times 3 \times 4$, and $8 \times 8 \times 3$ \mathbf{q} -points for $(4, 8^2)$, $(3, 12^2)$, (6^3) , and (4^4) 3D-Cs, respectively.

To examine the mechanically stable of the 3D-C ALs, we use the Thermo-pw code [32] to calculate the elastic constants C_{ij} . The calculated elastic constants are derived from the finite difference approach and are by default averaged over the entire unit cell volumes. From the point of view of elasticity theory, it is well-recognized that the value of C_{ij} is related to the equivalent volume of the crystal. To obtain the equivalent volume of the 3D-C ALs, the wall thickness, d , in the polygon vertices is considered as the interlayer spacing of graphite and multi-walled carbon nanotubes in nature based on the van der Waals interactions ($d = 3.4$ Å) [33], where d is assumed to be independent of the small strain and charge doping [14]. From the calculated C_{ij} , the polycrystalline corresponding bulk modulus B and shear modulus G are calculated using the Voigt-Reuss-Hill approximation [34], then Young's modulus E and Poisson's ratio

Table 1: Number of atoms in unit cell N , lattice parameters a (Å) and c (Å), and bond lengths (Å) of the 3D-C ALs.

Structure	N	a	c	$d_{sp^2-sp^2}$	$d_{sp^2-sp^3}$	$d_{sp^3-sp^3}$
$(4, 8^2)$	8	5.23	2.50	1.35	1.49	1.61
$(3, 12^2)$	12	8.13	2.51	1.36	1.47	1.56
(6^3)	16	6.34	4.82	1.38	1.49	1.63
(4^4)	6	2.60	5.98	1.37	1.54	-

ν are obtained by the following relations, $E = (9G \cdot B)/(3B + G)$, and $\nu = (3B - 2G)/(6B + 2G)$, respectively.

To discuss the electromechanical actuation of the 3D-C ALs, the geometry optimization is performed with the charge doping level, ranging from -0.15 to 0.15 electron per carbon atom, in which the electron (hole) doping is simulated by adding (removing) electrons to the unit cell with the same amount of uniformly positive (negative) charge in the background so as to keep the charge neutrality.

3. Results and Discussion

3.1. Structural properties

In Figs. 1a-c, we illustrate crystal structures of our proposed 3D-C ALs. Each AL is defined by a set of integers (p_1, p_2, \dots) indicating, in a unit cell, the type of polygons meeting at a given vertex (see Fig. 1a). When a polygon appears more than one time consecutively, e.g., (\dots, p, p, \dots) , we abbreviate the notation by writing (\dots, p^2, \dots) . For example, $(4, 8^2)$ 3D-C means that each vertex is surrounded sequentially by one square and two octagons, as shown in Figs. 1a and 1b. This property has made them useful in the study of mathematics [35], crystallization [36], as well as metamaterials [37]. Now, the designing principle of our 3D-C structures is that the polygon vertices are formed by diamond-like sp^3 bond, while the polygon edges consist of flattened sp^2 bond such like that in graphene sheets, as shown in Fig. 1b. For simplicity, we focus on four allotropes of the 3D-C ALs that are found to be stable theoretically, namely $(4, 8^2)$, $(3, 12^2)$, (6^3) , and (4^4) 3D-Cs. We note that some ALs such as $(3^4, 6)$ or $(3^2, 4, 3, 4)$ might not be suitable to be a 3D-C structure because the condition for the sp^3 bonding of carbon atom at each vertex is not satisfied [38]. The details of the crystal structures, including the number of atoms in unit cell, lattice parameters and bond lengths between sp^2 (green atoms) and sp^3 bonded atoms (red atoms), are shown in Table 1 and Fig. 1c.

3.2. Thermodynamics stability

In Fig. 2, we show the optimized total energy per carbon atom of the 3D-C ALs as a function of charge doping q ranging from -0.15 to 0.15 electron per carbon atom. This charge range is appropriate for our calculations because the limit of the experimentally accessible charge is 0.3 e/C-atom for graphite [13]. In the neutral condition, the total energy of the 3D-C ALs is close to that of C_{60} fullerene, 3D diamond, and

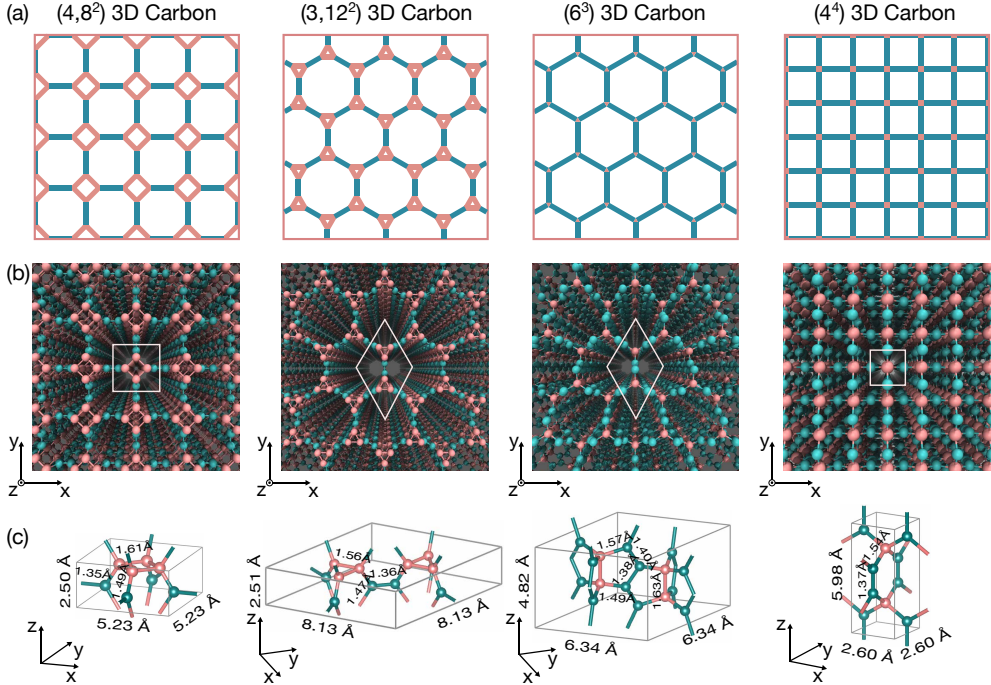


Figure 1: (a) The Archimedean lattices. (b) Perspective view of the 3D-C ALs structures in three-dimensional space. (c) The unit cell of the 3D-C ALs showing the lattice constants and the C-C bond lengths. Red atoms are sp^3 -hybridized, while green atoms are sp^2 -hybridized.

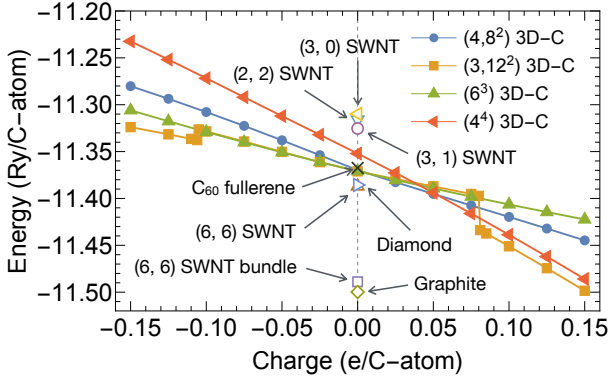


Figure 2: Optimized total energy per C-atom of the 3D-C ALs as a function of charge (electron and hole) doping per C-atom. At the charge $q = 0.00$ e/C-atom, total energies of individual (6, 6) SWNT [33], (6, 6) SWNT bundle [14], smallest carbon nanotubes including (2, 2), (3, 0) and (3, 1) SWNTs [33], graphite, diamond, C_60 fullerene are also calculated and plotted here for comparison.

individual (6, 6) single wall carbon nanotube (SWNT) [33]. On the other hand, the 3D-C ALs are less stable than (6, 6) SWNT bundle and graphite [14], but more stable than the smallest carbon nanotubes such as (2, 2), (3, 0) or (3, 1) SWNTs [33]. In fact, experimental evidence has shown that smallest SWNTs with diameters of about 0.4 nm exist as an inner core of multiwall carbon nanotubes and can also be found in the nanosize channels of porous materials [39, 40]. Moreover, Krainyukova et al. [22] have recently reported a stable 3D-C by the deposition of vacuum-sublimated graphite that points out to the possibility of obtaining a (6^3) 3D-C structure. These experimental

observations thus support a realization of the other 3D-C ALs in the near future. Of the four 3D-C ALs, the (4^4) 3D-C is the least stable, while the other 3D-C ALs have relatively similar energies, especially at the neutral condition. The total energy per atom in the 3D-C ALs monotonically decreases with increasing the charge doping except for the $(3, 12^2)$ 3D-C. In the case of $(3, 12^2)$ 3D-C, a finite jump of total energy per atom at electron ($q = -0.106$ e/C-atom) doping and hole ($q = 0.081$ e/C-atom) doping suggests sp^2 - sp^3 phases transformation, which will be discussed later based on the charge density calculation.

3.3. Dynamical and mechanical stability

In Fig. 3, we show phonon dispersions along the high-symmetry directions in the corresponding Brillouin zone of the four 3D-C ALs to discuss their lattice dynamics. All real phonon energies (positive eigenvalues from the Hessian matrix) confirm that the 3D-C ALs are dynamically stable. Three distinct acoustic modes including the in-plane longitudinal (LA), in-plane transverse (TA) and out-of-plane (ZA) modes exhibit linear dispersions near the Γ point, these modes are dominated by sp^2 bonding in the polygon edges. Note that, the ZA mode in the 3D-C ALs is unlike that in graphene sheet since the graphene ZA mode is quadratic dispersion [42]. The highest phonon frequency in 3D-C ALs reaches 1600 cm $^{-1}$, comparable to that in graphite [43] and diamond [44].

Next, we investigate the mechanical stability of the 3D-C ALs. To guarantee the positive strain energy during lattice distortion, the tensor components of the linear elastic constant (C_{ij}) of a stable crystal have to obey the Born criteria [45]. In the $(4, 8^2)$ and (4^4) 3D-Cs, there are six independent elastic con-

Table 2: Elastic constants C_{ij} (GPa), bulk modulus B (GPa), shear modulus G (GPa), Young's modulus Y (GPa), Poisson's ratio ν , and mass density ρ (g/cm³) of the 3D-C ALs, graphite, and diamond.

Structure	C_{11}	C_{33}	C_{44}	C_{66}	C_{12}	C_{13}	B	G	Y	ν	ρ
(4, 8 ²)	651	1026	260	30	90	67	303	179	449	0.25	2.33
(3, 12 ²)	372	1004	261	45	283	86	286	138	357	0.29	1.67
(6 ³)	346	1044	178	46	254	56	263	124	320	0.30	1.90
(4 ⁴)	704	1151	76	72	45	91	325	155	402	0.30	2.97
graphite ^a	1060	36	4	440	—	15	8	440	1020	0.16	2.30
diamond ^a	1070	1070	575	575	—	125	442	576	1063	0.10	3.63

^a Reference [21, 41].

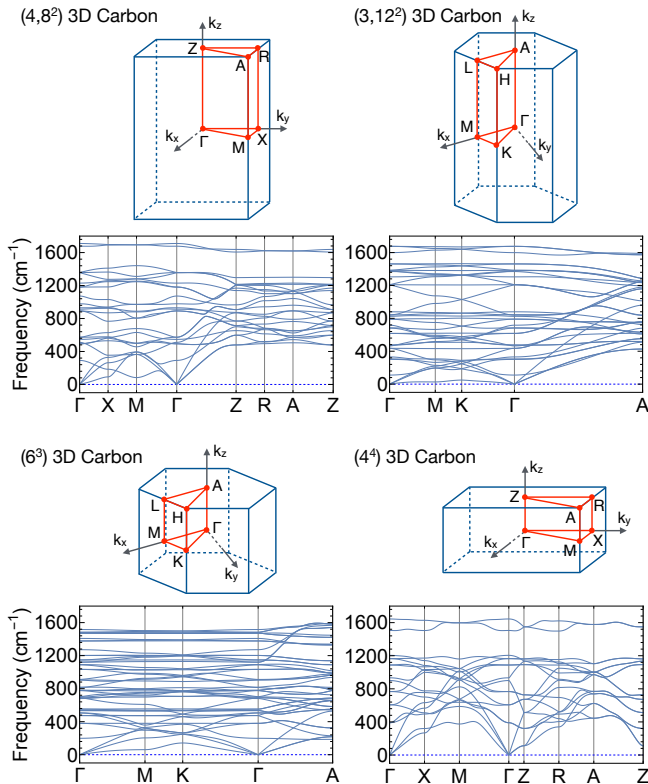


Figure 3: Phonon dispersions, high-symmetry points, and lines in the corresponding Brillouin zone of four different 3D-C ALs.

stants due to tetragonal symmetry, while in the (3, 12²) and (6³) 3D-Cs there are only five constants due to hexagonal symmetry, in which $C_{66} = (C_{11} - C_{12})/2$. According to the Born criteria, the elastic constants of the tetragonal and hexagonal crystals have to satisfy the following conditions [46]: $C_{11} > |C_{12}|$, $2C_{13}^2 < C_{33}(C_{11} + C_{12})$, $C_{44} > 0$, and $C_{66} > 0$ (the condition for C_{66} is redundant in the hexagonal case). The elastic constants can be derived by fitting the strain-stress curves associated with uniaxial and equibiaxial strains, as implemented in Thermo-pw code [32]. The calculated C_{ij} values of the 3D-C ALs are listed in Table 2 at the neutral charge. These constants obey all of the criteria above, indicating that all the four 3D-C ALs are mechanically stable.

3.4. Electronic properties

In Fig. 4, we show the calculated electronic structures of the 3D-C ALs along the high-symmetry directions in the corresponding Brillouin zone (see Fig. 3) for neutral and charge doping states. For the neutral case, we find that the (4, 8²) 3D-C is an indirect-gap semiconductor with a band gap of about 0.96 eV, the (3, 12²) 3D-C is a semimetal, while the (6³) and (4⁴) 3D-Cs are metals. The unusual electronic properties of the 3D-C ALs might originate from sp^2 and sp^3 bonded atoms (green and red atoms in Fig. 1) at the Fermi level. For the (6³) and (4⁴) 3D-Cs, the number of sp^3 bonded atoms is smaller than that of sp^2 bonded atoms in the unit cell. Therefore, most of the conducting electrons at the Fermi level are coming from the $2p_z$ orbitals of sp^2 bonded carbon atoms like that in graphene, which lead to the metallic properties of the (6³) and (4⁴) 3D-Cs. As for the (4, 8²) and (3, 12²) 3D-Cs, the numbers of sp^2 and sp^3 bonded atoms in the unit cell are the same. Therefore, both sp^2 and sp^3 bonded atoms contribute to the electrons at the Fermi level, which result in semiconducting (4, 8²) and semimetallic (3, 12²) 3D-Cs. Through a detailed analysis of the energy band structures under the charge doping, we can see that the energy bands change significantly under both heavy electron and hole dopings, which could affect the mechanical properties of the 3D-C ALs.

In Fig. 5, we show the energy band gap E_g as a function of charge doping q . For the semiconducting (4, 8²) 3D-C, E_g decreases with both electron and hole doping cases, leading to a semiconductor-to-metal transition at $q = \pm 0.15$ e/C-atom. For the semimetallic (3, 12²) 3D-C, a semimetallic-to-semiconductor transition occurs when q is adjusted up to 0.081 e/C-atom, while the (6³) and (4⁴) 3D-Cs retain their metallic states under charge doping. It is thus clear that the rigid band model, in which the effective mass and the band gap are fixed while Fermi level is shifted by charge doping, is not valid for the presented cases. As shown in Fig. 5, the rigid band model is remarkably more pronounced for the (3, 12²) 3D-C in both electron and hole dopings cases and for the (4, 8²) 3D-C in the electron doping case. For the (3, 12²) 3D-C, sp^3 bonded atoms break into sp^2 bonded atoms under heavy electron doping, while sp^2 bonded atoms make new sp^3 bonded atoms under heavy hole doping (see the charge density in Fig. 7). The energy band structure thus changes significantly, which leads to the metallic and semiconducting properties of the (3, 12²) 3D-C under heavy electron and hole dopings, respectively. For

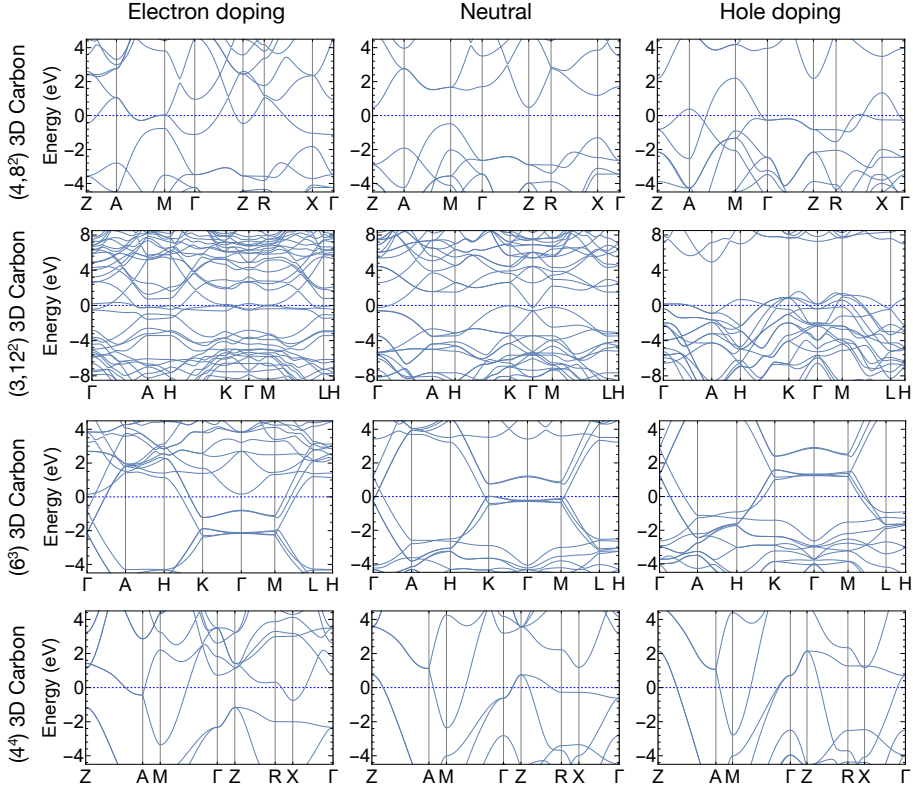


Figure 4: Energy band structures of the 3D-C ALs with different electron doping ($q = -0.15$ e/C-atom) and hole doping ($q = +0.15$ e/C-atom) including those with the neutral condition ($q = 0.00$ e/C-atom). The Fermi energy (dashed line) is set to zero for all plots.

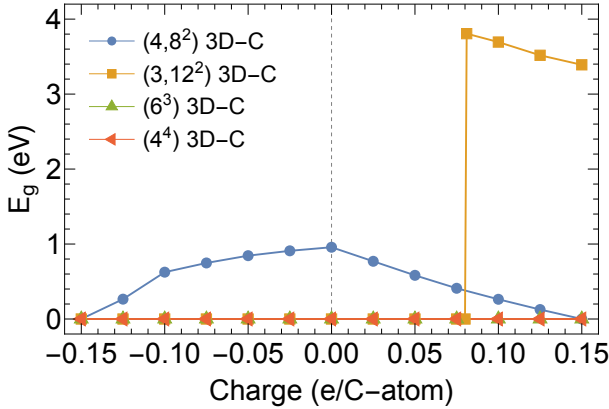


Figure 5: Energy band gap E_g plotted as function of charge doping of four different 3D-C ALs.

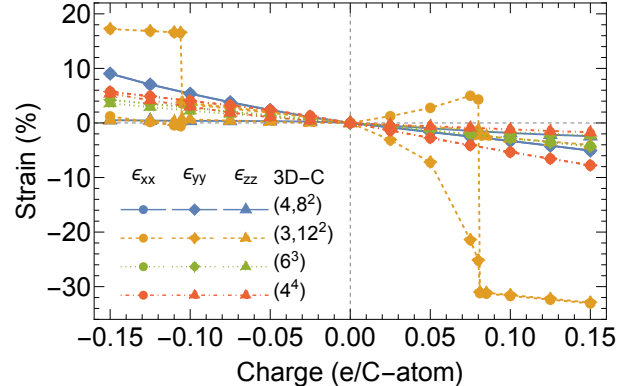


Figure 6: Strain as function of charge doping of four different 3D-C ALs.

3.5. Electromechanical properties

In Fig. 6, we show the charge-strain relationship of the 3D-C ALs. The strains of three 3D-C ALs, except the $(3, 12^2)$ 3D-C, are approximately a linear function of charge doping and are isotropic in $x - y$ plane. For the $(4, 8^2)$ 3D-C, $\varepsilon_{xx} = \varepsilon_{yy}$ is up to 9.0% (-5.1%) under the electron (hole) doping at $q = -0.15$ (0.15) e/C-atom, while $\varepsilon_{zz} = 0.5\%$ (2.4%). For the (6^3) 3D-C, $\varepsilon_{xx} = \varepsilon_{yy} = 4.2\%$ (-4.3%) and $\varepsilon_{zz} = 3.6\%$ (-2.3%) at $q = -0.15$ (0.15) e/C-atom. For the (4^4) 3D-C, $\varepsilon_{xx} = \varepsilon_{yy} = 5.7\%$ (-7.8%) and $\varepsilon_{zz} = 5.4\%$ (-1.7%) at $q = -0.15$ (0.15) e/C-atom.

the $(4, 8^2)$ 3D-C, its electromechanical response shows a higher strain value than the (6^3) and (4^4) 3D-Cs under heavy electron doping (see Sec. 3.5), which also leads to a significant change of the energy band structure. Therefore, the rigid band model is no longer suitable for the $(4, 8^2)$ 3D-C under heavy electron doping.

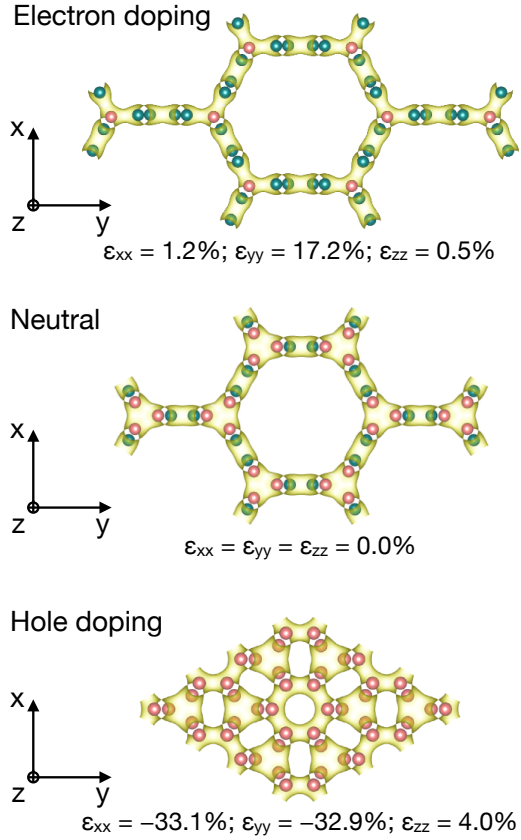


Figure 7: Charge density isosurface (0.13 e/a.u.^3) of the $(3, 12^2)$ 3D-C at neutral, heavy electron and hole dopings cases. Red atoms are sp^3 hybridized and blue atoms are sp^2 hybridized. At heavy electron and heavy hole doping regimes, the $(3, 12^2)$ 3D-C is transformed to (6^3) 3D-C and $(3, 4, 6, 4)$ 3D-C, respectively.

$e/\text{C-atom}$. As for the $(3, 12^2)$ 3D-C, the calculation results give an anisotropic strain under hole doping at $q = 0.08 \text{ e/C-atom}$ with ε_{xx} and ε_{yy} are up to 4.3% and -25.2%, respectively. For further hole doping, ε_{xx} and ε_{yy} show a finite jump that leads to $\varepsilon_{xx} = \varepsilon_{yy} \sim -31\%$ at $q = 0.081 \text{ e/C-atom}$. Similarly, for electron doping, ε_{xx} and ε_{yy} have a finite jump at $q = -1.06 \text{ e/C-atom}$ ($\varepsilon_{xx} = -0.6\%$ and $\varepsilon_{yy} = 16.5\%$). We argue that a very high strain of the $(3, 12^2)$ 3D-C under charge doping is a result of its chemical bond transformation. Based on the charge density plot in Fig. 7, sp^3 bonds change to sp^2 bonds under heavy electron doping, while sp^2 bonds change to sp^3 under heavy hole doping in the $(3, 12^2)$ 3D-C. However, these sp^2 - sp^3 transformations are not reversible. At heavy electron and heavy hole doping regimes, the $(3, 12)$ 3D-C is transformed to (6^3) 3D-C and $(3, 4, 6, 4)$ 3D-C, respectively. Nevertheless, the $(3, 12^2)$ 3D-C is a stable structure without charge doping.

To understand the stability of the 3D-C ALs under charge doping, the mechanical stability is investigated by the Born criteria [45] at different charge states. According to the Born criteria, the elastic constants C_{ij} of a stable 3D-C AL structure has to satisfy the conditions $C_{11} > |C_{12}|$, $2C_{13}^2 < C_{33}(C_{11} + C_{12})$, $C_{44} > 0$, and $C_{66} > 0$ (see Sec. 3.3). In Fig. 8, we calculate C_{ij} as a function of charge doping. We find that the $(4, 8^2)$, (6^3) and

(4^4) 3D-Cs are unstable under heavy hole doping because both C_{44} and C_{66} are less than zero, resulting in a negative strain energy. On the other hand, the $(3, 12^2)$ 3D-C is stable under both heavy electron and hole doping cases but its structure shows an irreversible sp^2 - sp^3 transformations under heavy charge doping (see Fig. 7). Having confirmed the stability of the 3D-C ALs, we then systematically study their mechanical properties.

Fig. 9a shows the bulk modulus B , the shear modulus G and Young's modulus Y of the *stable* 3D-C ALs as a function of charge doping. In Fig. 9, we omit some data points of heavy doping due to the instability of certain 3D-C ALs, i.e. they become distorted, at that regime. In the neutral condition, the $(4, 8^2)$ 3D-C has the highest $G = 179 \text{ GPa}$ and $Y = 449 \text{ GPa}$, while the (4^4) 3D-C has the highest $B = 325 \text{ GPa}$. Both G and Y are decreased, while B is increased by charge doping. In the case of a SWNT [33, 47], the axial Y is about 1 TPa, which is consistent with the in-plane Y of a graphene layer. However, the 3D structures of CNT composites, such as bundles, yarns, and fibers appear to be more flexible and elastic in their radial directions due to the weak van der Waals interactions between different tubes. The experimentally obtained Y values of CNT composites are only in the range of 0.35-80 GPa [48, 49, 50]. Compared with CNTs composites, the Y values of the 3D-C ALs are much higher by two order-of-magnitude. Therefore, our designed 3D-C ALs retain not only the superior mechanical performance in the axial directions of the tubes, but also give enhanced reinforcement in their radial directions through the sp^3 bond connections at the vertices of the 3D-C ALs. The large mechanical moduli of the 3D-C ALs are important for the artificial muscle application since it could generate large force per unit area.

Figure 9b shows Poisson's ratio ν of the *stable* 3D-C ALs as a function of charge doping. It is known that Poisson's ratio is a measure of the Poisson effect, a phenomenon in which a material tends to expand in the directions perpendicular to the direction of compression. In the neutral condition, the ν values of three 3D-C ALs are about 0.29, except for the $(4, 8^2)$ 3D-C which gives $\nu = 0.25$. These values are larger than those of SWNT ($\nu = 0.07 - 0.15$) and graphene ($\nu = 0.186$), which is suitable for muscle. In the 3D-C ALs, the Poisson effect is also further enhanced by the charge doping.

Finally, Fig. 9c shows the mass density ρ of the *stable* 3D-C ALs as a function of charge doping. At the neutral charge, (4^4) 3D-C has the highest $\rho = 2.97 \text{ g/cm}^3$ and $(3, 12^2)$ 3D-C has the lowest $\rho = 1.67 \text{ g/cm}^3$. These values are smaller than that of diamond (3.633 g/cm^3) and SWNT ($\sim 3.0 \text{ g/cm}^3$), and are close to that of graphite (2.295 g/cm^3) [21]. The low density of the 3D-C ALs is due to their porous structures along the axial z directions. Although the mass density of 3D-C ALs is higher than that of mammalian skeletal muscle ($\sim 1 \text{ g/cm}^3$), we expect that the designed 3D-C ALs with larger pore diameters along the z direction will give ultralow density. Pang et al., [51], for example, showed that the density of the (6^3) 3D-C can go down to 0.31 g/cm^3 with the pore diameter of about 29.7 \AA . However, both of the strength and failure strain decrease in (6^3) 3D-C with growing pore diameter [51]. We also note that for the 3D-C ALs with large pore diameter, the number of flattened sp^2 bonds at

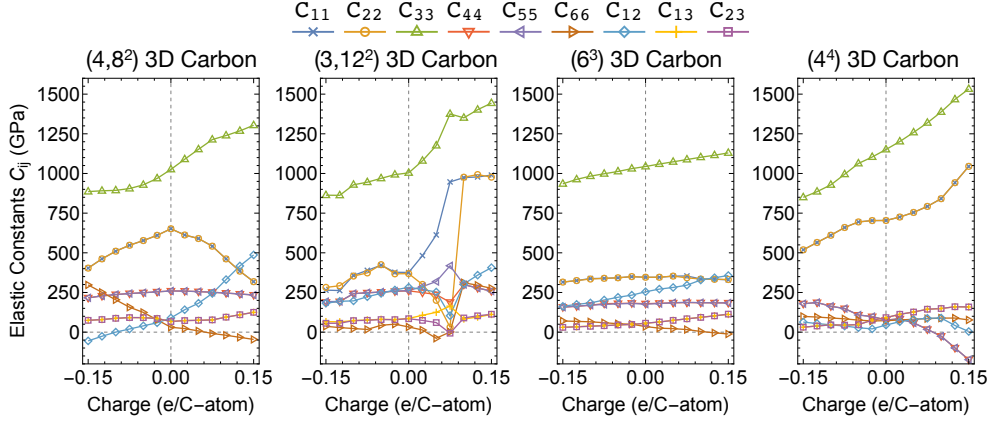


Figure 8: Elastic constants C_{ij} of four different 3D-C ALs plotted as function of charge (electron and hole) doping per carbon atom.

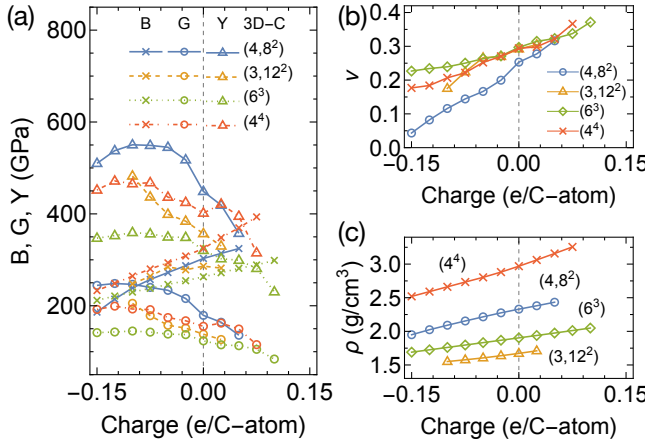


Figure 9: (a) Mechanical moduli, including the bulk modulus B , the shear modulus G , and Young's modulus Y , (b) Poisson's ratio ν , and (c) mass densities ρ of the 3D-C ALs plotted as function of charge doping. Note that we omit some data points of heavy doping due to the instability of certain 3D-C ALs at that regime.

the polygon edges is much higher than that of sp^3 bonds at the polygon vertices. Therefore, the 3D-C ALs might not be able to maintain their electromechanical properties when their pore diameters become larger.

4. Conclusions

By first principles DFT calculations, we have shown the feasibility of constructing stable 3D carbon materials based on the Archimedean lattices with excellent electromechanical properties. The reversible strain can be up to 9% with stable $(4,8^2)$ 3D-C structure under heavy electron doping, which is nine times larger than that of carbon nanotube or graphene. A very high irreversible strain of about 30% in the $(3,12^2)$ 3D-C is also found as a result of sp^2 - sp^3 bond transformation. Large mechanical moduli (including the bulk modulus, the shear modulus, and Young's modulus), large Poisson's effect, and low mass density under charge doping may be utilized

to obtain high-performance actuators with applications ranging from artificial muscle to biomedical engineering. Depending on the index of Archimedean lattices, the 3D-C ALs also show distinctive electronic properties: the $(4,8^2)$ 3D-C is an indirect band-gap semiconductor, the $(3,12^2)$ 3D-C is semimetal, while the (6^3) and (4^4) 3D-Cs are metals. Furthermore, we expect that the semiconductor-to-metal and semimetallic-to-semiconductor transitions found in the semiconducting $(4,8^2)$ and semimetallic $(3,12^2)$ 3D-Cs, respectively, under heavy charge doping will open further explorations of the 3D-C ALs in the near future.

Acknowledgments

N.T.H. and A.R.T.N acknowledge the Interdepartmental Doctoral Degree Program for Multidimensional Materials Science Leaders under the Leading Graduate School Program in Tohoku University. R.S. acknowledges JSPS KAKENHI Grant Numbers JP25107005 and JP25286005.

Supplementary information

Atomic coordinates (CIF files) of the optimized 3D-C ALs structures studied in this work.

References

- [1] R. H. Baughman, Playing nature's game with artificial muscles, *Science* 308 (5718) (2005) 63–65.
- [2] J. D. Madden, Artificial muscle begins to breathe, *Science* 311 (5767) (2006) 1559–1560.
- [3] T. Mirfakhrai, J. D. W. Madden, R. H. Baughman, Polymer artificial muscles, *Mater. Today* 10 (4) (2007) 30–38.
- [4] Y. Hu, W. Chen, L. Lu, J. Liu, C. Chang, Electromechanical actuation with controllable motion based on a single-walled carbon nanotube and natural biopolymer composite, *ACS nano* 4 (6) (2010) 3498–3502.
- [5] R. H. Baughman, C. Cui, A. A. Zakhidov, Z. Iqbal, J. N. Barisci, G. M. Spinks, G. G. Wallace, A. Mazzoldi, D. De Rossi, A. G. Rinzler, O. Jaschinski, S. Roth, M. Kertesz, Carbon nanotube actuators, *Science* 284 (1999) 1340–1344.

[6] J. Liang, Y. Huang, J. Oh, M. Kozlov, D. Sui, S. Fang, R. H. Baughman, Y. Ma, Y. Chen, Electromechanical actuators based on graphene and graphene/fe₃o₄ hybrid paper, *Adv. Funct. Mater.* 21 (2011) 3778–3784.

[7] Y. Huang, J. Liang, Y. Chen, The application of graphene based materials for actuators, *J. Mater. Chem.* 22 (2012) 3671–3679.

[8] G. W. Rogers, J. Z. Liu, Graphene actuators: quantum-mechanical and electrostatic double-layer effects, *J. Am. Chem. Soc.* 133 (2011) 10858–10863.

[9] G. W. Rogers, J. Z. Liu, High-performance graphene oxide electromechanical actuators, *J. Am. Chem. Soc.* 134 (2011) 1250–1255.

[10] G. Wu, Y. Hu, Y. Liu, J. Zhao, X. Chen, V. Whoehling, C. Plesse, G. T. M. Nguyen, F. Vidal, W. Chen, Graphitic carbon nitride nanosheet electrode-based high-performance ionic actuator, *Nat. Commun.* 6 (2015) 7258.

[11] J. Li, W. Ma, L. Song, Z. Niu, L. Cai, Q. Zeng, X. Zhang, H. Dong, D. Zhao, W. Zhou, S. Xie, Superfast-response and ultrahigh-power-density electromechanical actuators based on hierachical carbon nanotube electrodes and chitosan, *Nano Lett.* 11 (2011) 4636–4641.

[12] I. A. Levitsky, P. Kanelos, W. B. Euler, Electromechanical actuation of composite material from carbon nanotubes and ionomeric polymer, *J. Chem. Phys.* 121 (2004) 1058–1065.

[13] G. Sun, J. Kürti, M. Kertesz, R. H. Baughman, Dimensional changes as a function of charge injection in single-walled carbon nanotubes, *J. Am. Chem. Soc.* 124 (2002) 15076–15080.

[14] N. T. Hung, A. R. T. Nugraha, R. Saito, Charge-induced electrochemical actuation of armchair carbon nanotube bundles, *Carbon* 118 (2017) 278–284.

[15] R. Saito, G. Dresselhaus, M. S. Dresselhaus, *Physical Properties of Carbon Nanotubes*, Imperial College Press, London, 1998.

[16] N. Park, J. Ihm, Electronic structure and mechanical stability of the graphitic honeycomb lattice, *Phys. Rev. B* 62 (2000) 7614.

[17] X. L. Sheng, Q. B. Yan, F. Ye, Q. R. Zheng, G. Su, T-carbon: a novel carbon allotrope, *Phys. Rev. Lett.* 106 (2011) 155703.

[18] J. Y. Jo, B. G. Kim, Carbon allotropes with triple bond predicted by first-principle calculation: Triple bond modified diamond and t-carbon, *Phys. Rev. B* 86 (2012) 075151.

[19] L. Yang, H. Y. He, B. C. Pan, Theoretical prediction of new carbon allotropes, *J. Chem. Phys.* 138 (2013) 024502.

[20] K. Srinivasu, S. K. Ghosh, Electronic structure, optical properties, and hydrogen adsorption characteristics of supercubane-based three-dimensional porous carbon, *J. Phys. Chem. C* 116 (2012) 25015–25021.

[21] Z. Zhao, B. Xu, L. M. Wang, X. F. Zhou, J. He, Z. Liu, H. T. Wang, Y. Tian, Three dimensional carbon-nanotube polymers, *ACS Nano* 5 (2011) 7226–7234.

[22] N. V. Krainyukova, E. N. Zubarev, Carbon honeycomb high capacity storage for gaseous and liquid species, *Phys. Rev. Lett.* 116 (2016) 055501.

[23] H. Nishihara, Q. H. Yang, P. X. Hou, M. Unno, S. Yamauchi, R. Saito, J. I. Paredes, A. Martínez-Alonso, J. M. D. Tascón, Y. Sato, M. Terauchi, T. Kyotani, A possible buckybowl-like structure of zeolite templated carbon, *Carbon* 47 (2009) 1220–1230.

[24] P. Giannozzi, S. Baroni, N. Bonini, M. Calandra, R. Car, C. Cavazzoni, D. Ceresoli, G. L. Chiarotti, M. Cococcioni, I. Dabo, A. D. Corso, S. d. Gironcoli, S. Fabris, G. Fratesi, R. Gebauer, U. Gerstmann, C. Gougousis, A. Kokalj, M. Lazzeri, L. Martin-Samos, N. Marzari, F. Mauri, R. Mazzarello, S. Paolini, A. Pasquarello, L. Paulatto, C. Sbraccia, S. Scandolo, G. Scalauzero, A. P. Seitsonen, A. Smogunov, P. Umari, R. M. Wentzcovitch, Quantum espresso: a modular and open-source software project for quantum simulations of materials, *J. Phys. Condens. Matter* 21 (39) (2009) 395502.

[25] A. M. Rappe, K. M. Rabe, E. Kaxiras, J. D. Joannopoulos, Optimized pseudopotentials, *Phys. Rev. B* 41 (1990) 1227.

[26] We used the pseudopotentials from <http://www.quantum-espresso.org>.

[27] C. G. Broyden, The convergence of a class of double-rank minimization algorithms 1. general considerations, *IMA J. Appl. Math.* 6 (1970) 76–90.

[28] R. Fletcher, A new approach to variable metric algorithms, *Comput. J.* 13 (1970) 317–322.

[29] D. Goldfarb, A family of variable-metric methods derived by variational means, *Math. Comput.* 24 (1970) 23–26.

[30] D. F. Shanno, Conditioning of quasi-newton methods for function minimization, *Math. Comput.* 24 (1970) 647–656.

[31] S. Baroni, S. De Gironcoli, A. Dal Corso, P. Giannozzi, Phonons and related crystal properties from density-functional perturbation theory, *Rev. Mod. Phys.* 73 (2001) 515.

[32] A. Dal Corso, Elastic constants of beryllium: a first-principles investigation, *J. Phys. Condens. Matter* 28 (7) (2016) 075401.

[33] N. T. Hung, D. V. Truong, V. V. Thanh, R. Saito, Intrinsic strength and failure behaviors of ultra-small single-walled carbon nanotubes, *Comput. Mater. Sci.* 114 (2016) 167–171.

[34] O. L. Anderson, A simplified method for calculating the debye temperature from elastic constants, *J. Phys. Chem. Solids* 24 (1963) 909–917.

[35] J. Martinez, Archimedean lattices, *Algebra Univ.* 3 (1973) 247–260.

[36] H. Takeda, J. D. H. Donnay, Compound tessellations in crystal structures, *Acta Crystallogr.* 19 (1965) 474–476.

[37] D. Jovanović, R. Gajić, K. Hingerl, Refraction and band isotropy in 2d square-like archimedean photonic crystal lattices, *Opt. Express* 16 (2008) 4048–4058.

[38] R. Saito, Chapter 2 - hybrid orbital control in carbon alloys, in: E. Yusuda, M. Inagaki, K. Kaneko, M. Endo, A. Oya, Y. Tanabe (Eds.), *Carbon alloys*, Elsevier Science, 2003, pp. 15–40.

[39] L. C. Qin, X. Zhao, K. Hirahara, Y. Miyamoto, Y. Ando, S. Iijima, Materials science: The smallest carbon nanotube, *Nature* 408 (2000) 50–50.

[40] N. Wang, Z. K. Tang, G. D. Li, J. S. Chen, Materials science: Single-walled 4 Å carbon nanotube arrays, *Nature* 408 (2000) 50.

[41] J. P. Lu, Elastic properties of carbon nanotubes and nanoropes, *Phys. Rev. Lett.* 79 (1997) 1297.

[42] C. Si, W. Duan, Z. Liu, F. Liu, Electronic strengthening of graphene by charge doping, *Phys. Rev. Lett.* 109 (2012) 226802.

[43] J. Maultzsch, S. Reich, C. Thomsen, H. Requardt, P. Ordejón, Phonon dispersion in graphite, *Phys. Rev. Lett.* 92 (2004) 075501.

[44] J. L. Warren, J. L. Yarnell, G. Dolling, R. A. Cowley, Lattice dynamics of diamond, *Phys. Rev.* 158 (1967) 805.

[45] M. Born, K. Huang, *Dynamical theory of crystal lattices*, Clarendon Press, 1954.

[46] F. Mouhat, F. Coudert, Necessary and sufficient elastic stability conditions in various crystal systems, *Phys. Rev. B* 90 (2014) 224104.

[47] Y. Wu, M. Huang, F. Wang, X. M. H. Huang, S. Rosenblatt, L. Huang, H. Yan, S. P. O'Brien, J. Hone, T. F. Heinz, Determination of the youngs modulus of structurally defined carbon nanotubes, *Nano Lett.* 8 (2008) 4158–4161.

[48] T. Mirfakhrai, J. Oh, M. Kozlov, E. C. W. Fok, M. Zhang, S. Fang, R. H. Baughman, J. D. W. Madden, Electrochemical actuation of carbon nanotube yarns, *Smart Mater. Struct.* 16 (2007) S243.

[49] A. B. Dalton, S. Collins, E. Munoz, J. M. Razal, V. H. Ebron, J. P. Ferraris, J. N. Coleman, B. G. Kim, R. H. Baughman, Super-tough carbon-nanotube fibres, *Nature* 423 (2003) 703–703.

[50] J. N. Coleman, U. Khan, W. J. Blau, Y. K. Gun'ko, Small but strong: a review of the mechanical properties of carbon nanotube–polymer composites, *Carbon* 44 (2006) 1624–1652.

[51] Z. Pang, X. Gu, Y. Wei, R. Yang, M. S. Dresselhaus, Bottom-up design of three-dimensional carbon-honeycomb with superb specific strength and high thermal conductivity, *Nano Lett.* 17 (2017) 179–185.